Self-Assembled Materials

International Edition: DOI: 10.1002/anie.201502057
German Edition: DOI: 10.1002/ange.201502057

Coordination Assembly of Discoid Nanoparticles**

Kenji Hirai, Bongjun Yeom, Shu-Hao Chang, Hang Chi, John F. Mansfield, Byeongdu Lee, Sungsik Lee, Ctirad Uher, and Nicholas A. Kotov**

Abstract: *Supramolecular chemistry utilizes coordination bonds to assemble molecular building blocks into a variety of sophisticated constructs. However, traditional coordination assemblies are based on organic compounds that have limited ability to transport charge. Herein, we describe coordination assembly of anisotropic FeS_2 pyrite nanoparticles (NPs) that can facilitate charge transport. Zn^{2+} ions form supramolecular complexes with carboxylate end-groups on NP surface, leading to multiparticle sheets with liquid-crystal-like organization. Conductivity and Hall carrier mobility of the p-type layered semiconductor films with Zn^{2+} coordination bridging exceed those known for coordination compounds, some by several orders of magnitude. The nanoscale porosity of the assembled sheets combined with fast hole transport leads to high electrocatalytic activity of the NP films. The coordination assembly of NPs embraces the versatility of several types of building blocks and opens a new design space for self-organized materials combining nanoscale and supramolecular structural motifs.*

Supramolecular chemistry[1–3] and the self-assembly of nanoparticles (NPs)[4,5] are both used for the design of structurally complex materials for electronics, catalysis, solar cells, energy storage, and medicine, but otherwise have few intersection points.[6,7] Control of the nanoscale organization of self-assembled NP materials relies on intermolecular electrostatic,[8] van der Waals, hydrophobic, dipolar interactions,[5,9] hydrogen bonds[10,11] and entropic forces, whereas supramolecular materials are engineered by varying coordination linkages around metal ions. One could notice that coordination bonds are more powerful than many intermolecular forces.[12] Coordination assemblies also exemplify some of the most geometrically sophisticated superstructures that free-standing NP assemblies[10,11,13] still has to reach. These are compelling fundamental reasons for inclusion of coordination bonds into the palette of interactions controlling structural organization of NP constructs. Coordination assemblies of distinctly anisotropic NPs may also expand the concepts of coordination chemistry to include nanoscale structural segments capable of forming well-defined complexes with metal ions.

From the perspective of functionality, many biotic systems exploit coordination assemblies of organic building blocks and have attained exemplary performance in redox and photonic reactions optimized for the cellular environment.[14] Metal complexes can also lead to the preparation of continuous macroscale materials,[15,16] such as coordination polymers[17] and metal–organic frameworks,[18,19] which are associated with technologically exciting electronic, optical, and catalytic properties. At the same time, the organic building blocks known to permit electronic delocalization on the molecular scale may not be optimal for the nano-, meso-, and macroscale charge transport; for such applications NPs with semiconductor and metal properties may offer considerable advantages stemming from the nanoscale delocalization of electrons.

These fundamental and practical considerations inspired us to look into the possibility of NP assembly driven by interparticle coordination of metal ions. Our strategy for the coordination assembly of NPs was based on bridging the end-groups of organic stabilizers on the surface of NPs, for example, $-COO^-$ and $-NH_2$, which are capable of forming a variety of coordination complexes with metal ions. The interplay of the coordination bonds and non-covalent intermolecular interparticle interactions could lead to systems

[*] Dr. K. Hirai, Dr. B. Yeom, Dr. S.-H. Chang, Prof. Dr. N. A. Kotov
Department of Chemical Engineering, University of Michigan
Ann Arbor, MI 48109 (USA)
E-mail: kotov@umich.edu
Dr. B. Yeom
Department of Chemical Engineering, Myongji University
116 Myongji-ro, Cheoin-gu, Gyeonggi-do, 449-728 (South Korea)
Dr. H. Chi, Prof. C. Uher
Department of Physics, University of Michigan
Ann Arbor, MI 48109 (USA)
E-mail: cuher@umich.edu
Dr. J. F. Mansfield
Electron Microbeam Analysis Laboratory, University of Michigan
Ann Arbor, MI 48109 (USA)
Dr. B. Lee, S. Lee
Advanced Photon Source, Argonne National Laboratory
9700 S. Cass Avenue, Argonne, IL 60439 (USA)
Prof. Dr. N. A. Kotov
Department of Materials Science and Engineering, Department of Biomedical Engineering, and Biointerfaces Institute, University of Michigan, Ann Arbor, MI 48109 (USA)

[**] K.H. is grateful to JSPS Postdoctoral Fellowships for Research Abroad. The key parts of this work were supported by the NSF project "Energy- and Cost-Efficient Manufacturing Employing Nanoparticles" (NSF 1463474 to N.A.K.). Partial support was also made by the Center for Photonic and Multiscale Nanomaterials (C-PHOM) funded by the National Science Foundation (NSF) Materials Research Science and Engineering Center program DMR 1120923 as well as NSF projects 1403777 and 1411014. We thank the University of Michigan's EMAL for its assistance with electron microscopy, and for the NSF grant DMR-9871177 for funding of the JEOL 2010F analytical electron microscope used in this work. We are also grateful to the X-ray MicroAnalysis Laboratory (XMAL) for assistance with the use of Bruker XRD instrument and the Department of Chemistry for assistance with the ICP-OES. Use of the Advanced Photon Source, an Office of Science User Facility operated for the US Department of Energy (DOE) Office of Science by Argonne National Laboratory, was supported by the US DOE.
Supporting information for this article is available on the WWW under http://dx.doi.org/10.1002/anie.201502057.

with non-random distributions of nanoscale building blocks, especially in the case of anisotropic NPs.

To evaluate this hypothesis, we used pyrite NPs stabilized with thioglycolic acid (TGA). These NPs have a discoid shape with an average diameter of 4.0 ± 0.8 nm (Figure 1 a,d) and average height of 1.2 ± 0.4 nm (Figure 1 c,d) as determined by transmission electron microscopy (TEM) and atomic force microscopy (AFM), respectively. The observed 0.54 nm lattice spacing corresponds to the bc lattice planes of pyrite (Figure 1 b) and indicates that the a axis is oriented along the surface normal to the top/bottom faces of the discoid NPs with atomic structure described in Figure 1 e.

To form coordination complexes, 12 mg L^{-1} aqueous dispersions of FeS_2 NPs were mixed with aliquots of 10 mM $ZnCl_2$. For most experiments, pH was maintained at 6, at which Zn^{2+} is known to form coordination bonds with carboxylate groups. After 12–48 h of incubation at room temperature, we observed formation of a black precipitate (Figure 2 a,b) that consisted of irregularly shaped nanoscale sheets with a lateral dimension of 80–300 nm and rather uniform thickness of 10–20 nm (Figure 2 b,c). TEM tomography confirmed their planar geometry and visualized the granular morphology of the sheets expected for NP-based structures assembled from individual nanoscale units (Figure 2 d).[20] The pores between the NPs in the nanosheets are 6–10 nm.

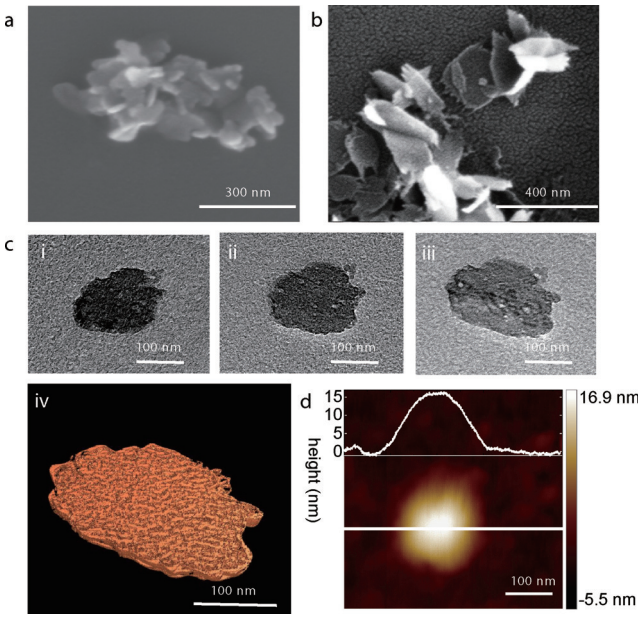

Figure 2. a,b) SEM images of the assembly product obtained after a) 12 h and b) 48 h incubation. c) TEM tomography of assembled nanosheets; TEM images of the nanosheet for viewing angles of i) −70°, ii) 0°, iii) +70°, iv) 3D surface rendering of the assembled nanosheets. d) AFM image of the individual particle of the assembly product.

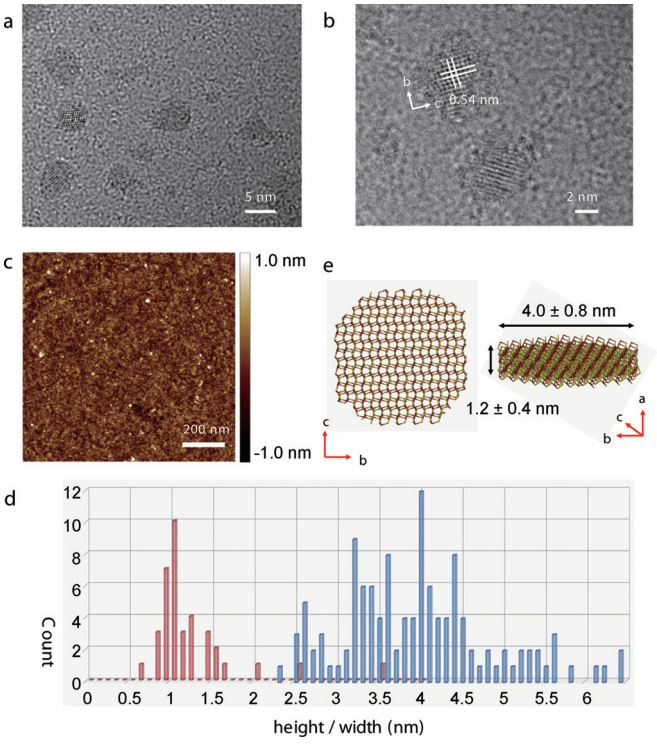

Figure 1. a,b) TEM images of TGA-stabilized FeS_2 NPs. The crystalline lattice of the bc plane can be seen. c) AFM image of TGA-stabilized NPs deposited on a silicon wafer. d) The statistical distribution of NP heights (red) and diameters (blue) determined from AFM and TEM images, respectively. e) Model atomic structure of the discoid FeS_2 NP. TGA stabilizers are omitted for clarity. The brown and yellow junctions indicate iron and sulfur atoms, respectively.

The XRD pattern of the assembled nanosheets corresponded to pyrite (JCPDS 00-042-1340, Figure S1a,b,d in the Supporting Information (SI)); no XRD peaks characteristic of other materials, for example, ZnS, were observed. Energy dispersive X-ray spectroscopy (EDX) (Figure 3 a and S2) showed that along with iron and sulfur, zinc atoms were also present in the nanoscale assembly products. IR spectroscopy of the original FeS_2 NPs revealed an IR band at 1690 cm^{-1} corresponding to the stretching vibration of a free carbonyl group of the TGA surface ligand. After the reaction with $ZnCl_2$, this IR band split into the symmetric 1470 cm^{-1} and anti-symmetric 1620 cm^{-1} vibrations (Figure 3 b) indicative of the formation of the coordination bond between carboxylate groups and Zn^{2+}. Synchrotron extended X-ray absorption fine structure spectroscopy (EXAFS) helped us establish the coordination pattern of Zn^{2+} and the supramolecular geometry of the interparticle bridges. The radial distribution function of Zn^{II} in the nanoscale sheets was found to be nearly identical to that of $[Zn_4(\mu_4\text{-}O)]^{6+}$ supramolecular clusters (Figure S3) in zinc stearate. The interparticle bridges have, therefore, quite intricate atomic structure. They are based on tetrahedrons from four Zn^{2+} ions "caged" by six carboxylate end-groups from TGA ligands. Three of carboxylates are likely belong to one NP and three on the opposite side of the complex belong to the other one. The possibility of partial inclusion of free TGA molecules in the structure of the supramolecular bridges should be considered.

Thus, a range of experimental data sets are consistent with the assembly of the NPs into nanosheets driven by coordination bonds between the particles rather than by van der Waals forces, hydrogen bonds, recrystallization, or oriented attach-

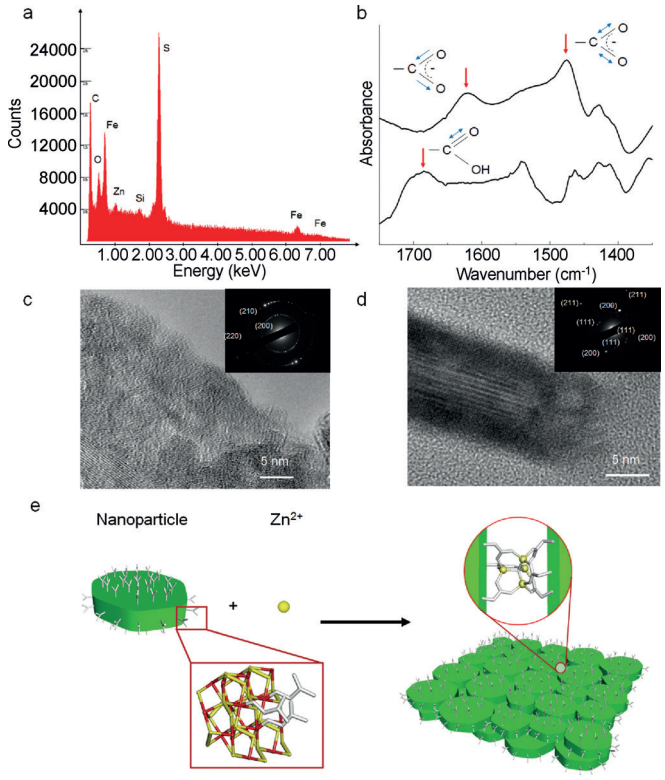

Figure 3. a) EDX spectrum of the assembled NP sheets. b) IR spectra of the assembled nanosheets (top) and original FeS_2 NPs (bottom). The arrows indicate the stretching vibration of carbonyl group (1690 cm^{-1}), the symmetric and anti-symmetric vibrations of carboxylate (1470 cm^{-1} and 1620 cm^{-1}). c, d) TEM images and ED (insets) of the nanosheets in the directions parallel c) and perpendicular d) to the discoid's normal. e) Schematic illustration of the coordination assembly of NPs. NPs are linked by $[Zn_4(\mu_4\text{-}O)]^{6+}$ supramolecular clusters involving six carboxylates from TGA.

ment.[21] This conclusion can be further affirmed by the observation of disassembly of the self-organized nanosheets into original discoid NPs. The Zn^{2+}-based coordination bridges were broken by addition of 1 M of an aqueous solution of tetrasodium ethylenediaminetetraacetate (EDTA), after which NPs identical in size and shape to the original ones were recovered (Figure S4).

Electron diffraction (ED) allowed us to better understand the mutual orientation the FeS_2 disks in the assembled nanosheets. ED patterns taken with an electron beam penetrating in the direction of normal to the face of the discoids revealed 200, 210, and 220 pyrite reflections (Figure 3c and Figure S5). ED patterns in the perpendicular direction taken from the edges of sliced nanosheets showed additional reflections from the 111 and 211 planes (Figure 3d). Cumulatively the ED data suggest that the planes of discoids are oriented parallel to the planes of nanosheets stacked on top of each other (Figure 3e). Confirming this attribution, a broad peak with $q \approx 0.1$ associated with the spacing between discoid NPs in the plane of the nanosheets was observed in the synchrotron small angle X-ray scattering (SAXS) and more clearly in the fitted structure factor, suggesting $d = 6.2$ nm (Figure S6). This distance matches well with the sum of the average diameter of FeS_2 discoids (4 nm) and the calculated dimensions of the $[Zn_4(\mu_4\text{-}O)](TGA)_6$ bridge (1.2 nm). The width of SAXS peak reflects the diameter distribution of the discoids.

Despite past observations of assembled NP sheets,[20,22] the spontaneous layering of pyrite NPs in these template-free assembled superstructures was a surprise to us. First of all, our a priori expectations about the products from coordination cross-linking of irregularly shaped discoid NPs (Figure 1a) would be disorganized aggregates. Instead, coordination bonds in combination with other interactions showed the ability to produce stacks of well-aligned particles and consistent liquid-crystal-like order. Second, the average thickness of assembled nanosheets (Figure 2) implies that 5–10 pyrite NPs are stacked together in the face-to-face configuration. Concomitantly, the lateral dimensions of the nanosheets imply that 20–70 NPs are bridged together in the edge-to-edge configuration. Despite expectations of greater probability of $[Zn_4(\mu_4\text{-}O)]^{6+}$ formation for basal surfaces of the discoids due to a higher density of stabilizers and proximal positioning of partner carboxylate ligands, coordination bridging of discoid NPs in the edge-to-edge geometry was experimentally shown to be more favorable than that in the face-to-face or side-to-face geometries (Figure S7).

The spontaneous assembly of free-standing nanosheets with these counterintuitive patterns is attributed to the electrostatic interactions between the individual NPs. After coordination of Zn^{2+} by the TGA carboxylate groups, the NPs acquire high positive charge (Figure S8). Electrostatic repulsion along the discoid normal results in self-limited nanosheet thickness similarly to self-limited supraparticle diameters assembling from isotropic NPs.[23] Consequently, the nanosheet thicknesses of the assemblies are fairly uniform whereas the lateral dimensions are not. Besides electrostatic interactions, the effect of NP curvature on pK_a of TGA ligands (SI) favoring coordination at the edges rather than on the basal surfaces may also facilitate edge-to-edge attachment pattern.

Coordination bonds between NPs bridged by Zn^{2+} ions are presumably affected by pH, concentration, temperature, and the chemical nature of the metal ions. Detailed accounts of experiments testing different media effects as well as different metal ions (Na^+, Ca^{2+}, Mn^{2+}, Cu^{2+}, and Ru^{2+}) are included in Figures S9–S12. The observations in all these experimental series are consistent with coordination bonds being the driving force for the formation of the TGA-stabilized NPs. They also allow us to predict generality of coordination assembly of FeS_2 and other NPs capable of forming supramolecular NP bridges.

In order to investigate charge transport in the coordination assemblies of pyrite NPs and their transition to application-friendly thin macroscale films, we combined coordination assembly of NPs with layer-by-layer deposition (LBL or LbL) (Figure 4a), enabling the preparation of continuous NP coatings on conducting and insulating supports. This kind of coordination assembly will be denoted here as $(NP/Zn^{2+})_n$, where n is the number of LBL deposition cycles (Figure 4b).[24,25] We observed that intensity of the UV/Vis spectra of $(NP/Zn^{2+})_n$ gradually increased with increasing n. The appearance of a distinct new spectral feature at 390 nm compared to free NPs should be noted (Figure S15). Similarly

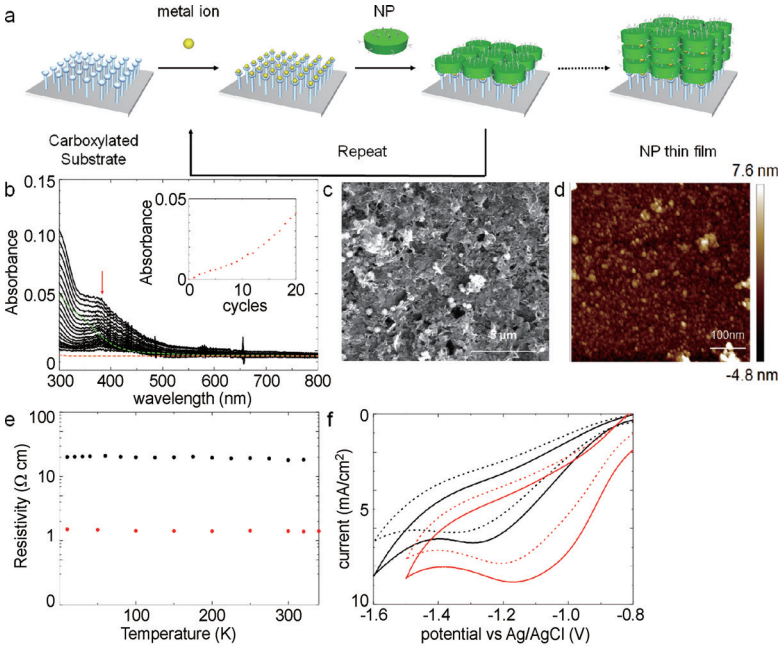

Figure 4. a) Schematic illustration of LBL deposition using coordination assembly. Several NP layers can potentially be adsorbed in one deposition cycle. b) UV/Vis spectra of LBL-deposited films obtained for $n = 1$–20. The green and orange dotted lines indicate UV/Vis spectra of NPs and the Zn-TGA complex, respectively. UV/Vis absorbance of $(NP/Zn^{2+})_n$ at 390 nm for different n values (inset). c,d) SEM and AFM images of a $(NP/Zn^{2+})_{200}$ film. e) Temperature-dependence resistivity of $(NP/Zn^{2+})_{200}$ (red) and drop-cast NP films (black). f) Cyclic voltammograms of $(NP/Zn^{2+})_{200}$ under light (red solid), drop-cast NP film (black solid) under light, $(NP/Zn2+)_{200}$ in dark (red dots), drop-cast NP film in dark (black dots).

to assemblies in dispersion, EDX spectroscopy showed that the film contained Fe, S, and Zn atoms (Figure S13). AFM imaging indicated that the discoid NPs were oriented parallel to the substrate (Figure 4c). The observed change from self-limited to continuous growth of the coordination assemblies for $(NP/Zn^{2+})_n$, while retaining the organization of platelets similar to that in free-standing assemblies in solution, is associated with the cyclic alteration of surface charge typical for LBL deposition.

The conductivity of $(NP/Zn^{2+})_{200}$ increase with temperature, as expected for semiconductors. Hall effect measurements for $(NP/Zn^{2+})_{200}$ indicated p-type conductivity (Figure S14) characteristic of pyrite films (Table S2). The conductivity at 300 K for $(NP/Zn^{2+})_{200}$ was $\sigma = 0.716\ S\,cm^{-1}$. The influence of coordination assembly on the electrical properties of the film can be assessed by comparing $(NP/Zn^{2+})_{200}$ with films in which NPs were not bridged by Zn^{2+} ions. As such, drop-cast NP films showed a value of $\sigma = 0.0728\ S\,cm^{-1}$(Figure 4e), 10 times smaller than that observed for $(NP/Zn^{2+})_{200}$. The carrier mobility (μ_h) and carrier density (n_h) of $(NP/Zn^{2+})_{200}$ were $\mu_h = 19\ cm^2V^{-1}s$ and $n_h = 2.2 \times 10^{17}\ cm^{-3}$, which is at least one order of magnitude higher than those observed for drop-cast NP films with $\mu_h = 2.1\ cm^2V^{-1}s$, $n_h = 2.0 \times 10^{17}\ cm^{-3}$. These experiments indicate that hole transfer between NPs becomes more facile after coordination bridging. This finding correlates well with facilitation of electron transport after covalent bridging of NPs.[26] Significant improvements in charge transport are seen in comparison with coordination polymers with σ from 10^{-8} to $0.2\ S\,cm^{-1}$ (Table S3). The corresponding values for coordination assemblies of NPs exceed many of these by several orders of magnitude, which can be attributed to the use of inorganic NPs as building blocks for the self-assembled materials. Further improvements can be expected with optimization of the length and molecular structure of NP stabilizing ligand.

The practical significance of NP films is often associated with solution processing of electronic devices. In this perspective, p-type semiconductor films with high hole mobility are indeed rare and highly sought-after in order to complement n-type solution-processed nanomaterials (Table S2). Besides that, p-type semiconductor NP films are valuable for electrocatalysis and photocatalysis.[27] These chemical processes are essential for a broad spectrum of environmental/energy technologies represented by synthesis of numerous organic compounds, fuel cells, reduction of CO_2, reactive superadsorbers, and pollution control.[28] The interparticle connectivity of the coordination assemblies, their supramolecular catalytic sites and nanoscale porosity (Figure 2d) are important structural assets for the design of photo- and electrocatalysts. Thus, we decided to test the electrocatalytic performance of $(NP/Zn^{2+})_{200}$ using benzyl chloride reduction, which often serves as a benchmark reaction for coordination compounds (Table S4). The cyclic voltammogram (Figure 4f) of $(NP/Zn^{2+})_{200}$ indicated high catalytic activity with reduction potential of benzyl chloride at E_r, dark $= -1.20$ V. This value is lower than those obtained for drop-cast FeS_2 NPs ($E_r = -1.32$ V) and other films, indicating more facile charge transfer to the substrate. An increase of reductive current under illumination (Figure S16) indicated that the photon energy can potentially assist the reduction process in our system. Indeed, a further decrease of reduction potential to E_r, light $= -1.13$ V was observed under illumination of $(NP/Zn^{2+})_{200}$ at the maximum of the absorption band in Figure 4b. This value is lower than that obtained for drop-cast FeS_2 NPs (E_r, light $= -1.32$ V), and other coordination compounds. Some of these, such as [Co(salen)], were designed specifically for electrocatalysis (Table S4).

The coordination of NPs by metal ion bridges represents a versatile methodology for the self-assembly of nanomaterials. The technique offers tremendous variability of the building blocks, that is, NPs, their stabilizing ligands with different coordination sites, and metal ions. The interplay of the three-dimensional orientation of coordination bonds with the anisotropy of interparticle interactions at the nanoscale can lead to unique assembly patterns. Importantly, coordination assembly of NPs affords pore sizes/geometries that are sometimes possible but challenging to obtain with zeolites, MOFs,[2,8,19,29] and DNA-based constructs.[30] Besides the

catalytic/electronic functionalities of coordination assemblies of NPs discussed here, other areas of chemistry and materials science, for example, ion transport and gas phase chemistry, are expected to benefit from the structural synergy between NPs and metal coordination complexes.

Keywords: conductive materials · coordination bond · nanoparticles · supramolecular assemblies

How to cite: *Angew. Chem. Int. Ed.* **2015**, *54*, 8966–8970
Angew. Chem. **2015**, *127*, 9094–9098

[1] J.-M. Lehn, *Science* **2002**, *295*, 2400–2403.
[2] M. Fujita, *Chem. Soc. Rev.* **1998**, *27*, 417–425.
[3] D. Philp, J. Stoddart, *Angew. Chem. Int. Ed. Engl.* **1996**, *35*, 1154–1196; *Angew. Chem.* **1996**, *108*, 1242–1286.
[4] E. Shevchenko, D. Talapin, N. A. Kotov, S. O'Brien, C. Murray, *Nature* **2006**, *439*, 55–59.
[5] a) Z. Tang, N. A. Kotov, *Science* **2002**, *297*, 237–240; b) T. Ni, D. K. Nagesha, J. Robles, N. Materer, S. Müssig, N. A. Kotov, *J. Am. Chem. Soc.* **2002**, *124*, 3980—3992.
[6] M. Yuan, D. Zhitomirsky, V. Adinolfi, O. Voznyy, K. W. Kemp, Z. Ning, X. Lan, J. Xu, J. Y. Kim, H. Dong, E. H. Sargent, *Adv. Mater.* **2013**, *25*, 5586–5592.
[7] S. Satyabrata, A. Kotal, T. K. Mandal, *J. Phys. Chem. C* **2007**, *111*, 1248–1255.
[8] A. M. Kalsin, M. Fialkowski, M. Paszewski, S. K. Smoukov, K. J. M. Bishop, B. A. Grzybowski, *Science* **2006**, *312*, 420–424.
[9] a) D. V. Talapin, E. V. Shevchenko, *Nano. Lett.* **2007**, *7*, 1213–1219; b) S. Shanbhag, N. A. Kotov, *J. Phys. Chem. B* **2006**, *110*, 12211—12217.
[10] D. Nykypanchuk, M. M. Maye, D. van der Lelie, O. Gang, *Nature* **2008**, *451*, 549–552.
[11] S. Y. Park, A. K. Lytton-Jean, B. Lee, S. Weigand, G. C. Schatz, C. A. Mirkin, *Nature* **2008**, *451*, 553–556.
[12] B. L. Vallee, D. S. Auld, *Biochemistry* **1990**, *29*, 5647–5659.
[13] S. Srivastava, A. Santos, K. Critchley, K.-S. Kim, P. Podsiadlo, K. Sun, J. Lee, C. Xu, G. D. Lilly, S. C. Glotzer, N. A. Kotov, *Science* **2010**, *327*, 1355–1359.
[14] N. J. Sanghamitra, T. Ueno, *Chem. Commun.* **2013**, *49*, 4114–4126.
[15] S. Takaishi, M. Hosoda, T. Kajiwara, H. Miyasaka, M. Yamashita, Y. Nakanishi, Y. Kitagawa, K. Yamaguchi, A. Kobayashi, H. Kitagawa, *Inorg. Chem.* **2009**, *48*, 9048–9050.
[16] A. A. Talin, A. Centrone, A. C. Ford, M. E. Foster, V. Stavila, P. Haney, R. A. Kinney, V. Szalai, F. El Gabaly, H. P. Yoon, F. Léonard, M. D. Allendorf, *Science* **2014**, *343*, 66–69.
[17] B. F. Hoskins, R. Robson, *J. Am. Chem. Soc.* **1990**, *112*, 1546–1554.
[18] S. Kitagawa, R. Kitaura, S. Noro, *Angew. Chem. Int. Ed.* **2004**, *43*, 2334–2375; *Angew. Chem.* **2004**, *116*, 2388–2430.
[19] M. Eddaoudi, J. Kim, N. Rosi, D. Vodak, J. Wachter, M. O'Keeffe, O. M. Yaghi, *Science* **2002**, *295*, 469–472.
[20] Z. Tang, Z. Zhang, Y. Wang, S. C. Glotzer, N. A. Kotov, *Science* **2006**, *314*, 274–278.
[21] C. Schliehe, B. H. Juarez, M. Pelletier, S. Jander, D. Greshnykh, M. Nagel, A. Meyer, S. Foerster, A. Kornowski, C. Klinke, H. Weller, *Science* **2009**, *329*, 550–553.
[22] A. Dong, J. Chen, P. M. Vora, J. M. Kikkawa, C. B. Murray, *Nature* **2010**, *466*, 474–477.
[23] J. I. Park, T. D. Nguyen, G. de Queirós Silveira, J. H. Bahng, S. Srivastava, G. Zhao, K. Sun, P. Zhang, S. C. Glotzer, N. A. Kotov, *Nat. Commun.* **2014**, *5*, 3593.
[24] G. Decher, *Science* **1997**, *277*, 1232–1237.
[25] O. Shekhah, H. Wang, T. Strunskus, P. Cyganik, D. Zacher, R. Fischer, C. Wöll, *Langmuir* **2007**, *23*, 7440–7442.
[26] M. V. Kovalenko, M. Scheele, D. V. Talapin, *Science* **2009**, *324*, 1417–1420.
[27] A. B. Bocarsly, Q. D. Gibson, A. J. Morris, R. P. L'Esperance, Z. M. Detweiler, P. S. Lakkaraju, E. L. Zeitler, T. W. Shaw, *ACS Catal.* **2012**, *2*, 1684–1692.
[28] H. Kim, C. Lee, *Angew. Chem. Int. Ed.* **2012**, *51*, 12303–12341; *Angew. Chem.* **2012**, *124*, 12469–12472.
[29] J. Liu, B. Lukose, O. Shekhah, H. K. Arslan, P. Weidler, H. Gliemann, S. Bräse, S. Grosjean, A. Godt, X. Feng, K. Müllen, I.-B. Magdau, T. Heine, C. Wöll, *Sci. Rep.* **2012**, *2*, 921.
[30] E. Winfree, F. Liu, L. A. Wenzler, N. C. Seeman, *Nature* **1998**, *394*, 539–544.

Received: March 4, 2015
Published online: June 11, 2015

